Hindawi
International Journal of Antennas and Propagation
Volume 2022, Article ID 2011410, 10 pages
https://doi.org/10.1155/2022/2011410

Research Article

Parasitic Elements Shorted to Ground to Enhance the Bandwidth of a Dual-Polarized Antenna

Haokai Jia,[1] **Jinjun Mo**,[2] **and Lin Peng**[1]

[1]*The Key Laboratory of Microwave and Optical Wave Application Technology, Guilin University of Electronic Technology, Guilin, China*
[2]*Guangxi Key Laboratory of Wireless Wideband Communication and Signal Processing, Guilin University of Electronic Technology, Guilin, China*

Correspondence should be addressed to Jinjun Mo; jinjunmo@guet.edu.cn

Received 25 April 2022; Revised 12 July 2022; Accepted 16 July 2022; Published 9 August 2022

Academic Editor: Miguel Ferrando Bataller

An ultra-wideband dual-polarized antenna covering multiple communication standards such as LTE700/GSM850/GSM900 is proposed in this paper. The antenna consists of two dipoles that are perpendicularly placed to each other. The two dipoles can generate +45°/−45° linear polarizations, respectively. Dual-loop structure is utilized as the arm of the dipole, while four parasitic patches with shorting walls are coupled to the dipoles to extend the operating bandwidth. The measured results show that the antenna has an impedance bandwidth of 101.4% (0.54 GHz–1.65 GHz) with a reflection coefficient less than −10 dB. The isolation between the two ports is larger than 22 dB, and the cross-polarization is less than −20 dB over the band. Good unidirectional radiation patterns are obtained.

1. Introduction

The UHF band is mostly utilized for military communications, ground-penetrating radar, and security detection because of its high anti-interference capability, high penetration, and low transmission loss [1]. Dual-polarized antennas are widely used in base stations and emergency communications due to their ability to double the channel capacity of communication systems [2–5]. Especially, cities and towns are full of high-rise buildings, and then, +45°/−45° dual-polarized antennas are needed to effectively suppress multipath effects and improve the communication performances. Besides, the ultra-wideband characteristic is required to supply high data rates and to cover different frequency regimes. Therefore, the study of ultra-wideband, low profile +45°/−45° dual-polarized antennas is of great significance.

Many different types of wideband dual-polarized antennas have been proposed in recent years, such as self-grounded antennas [6, 7] and planar-printed dipole antennas [8–17]. The former is usually compact and has ultra-wideband characteristics; however, its high profile and complicated structure make an obstacle in practical applications. The planar dipole antennas have simple structure. Many methods were utilized to achieve ultrawideband for planar dipole antennas. The first method is to improve the feeding structure, such as stepped microstrip feedlines [10], baluns [11], and differential feeding [12]. The second method is to optimize the antenna structure, such as slot loading to excite different resonant modes [9–11, 13]. The third method is to introduce parasitic elements on the antenna to extend the current path [14, 15]. In [16, 17], by loading metal plates, antennas achieve operating bandwidths of 49% and 92%, respectively.

In this paper, an ultra-wideband dual-polarized antenna with parasitic elements is proposed. The impedance bandwidth of the antenna is enhanced through the coupling between the dipoles and the shorting metallic plates. The structure and working principle of the antenna are discussed in Section 2. The simulated and measured results are presented in Section 3.

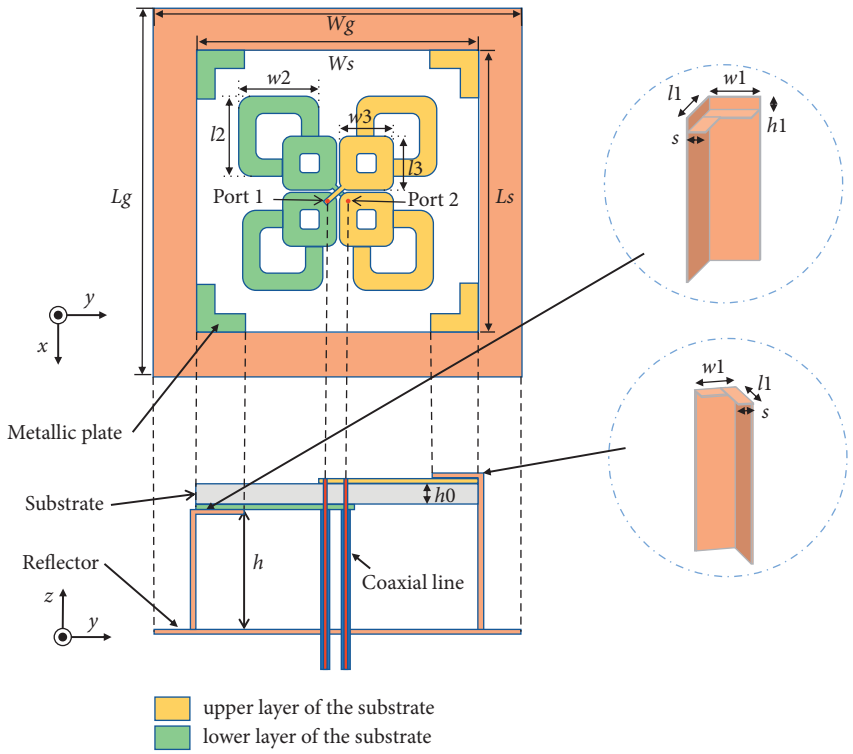

Figure 1: Configuration of the ultra-wideband dual-polarized antenna.

2. Antenna Design and Operating Principle

2.1. Antenna Design and Discussion. Figure 1 shows the configuration of the proposed wideband dual-polarized dipole antenna. The proposed antenna consists of four double-loop structures and four parasitic elements. Two square loops of different sizes are used to form a double-loop structure. The two double-loop structures of one dipole are printed on the front and back sides of the dielectric substrate (FR-4, ε_r = 4.4 and thickness = 2 mm). A parasitic element consists of a parasitic L-shaped patch, which is soldered by an L-shaped metallic shorting wall. The strong coupling between the double-loop structure and the parasitic element generates new resonance, which effectively expands the bandwidth to lower frequency. For the dipole with −45° polarization, the outer conductor of the coaxial line is connected to the double-loop structure printed on the back side of the substrate, and the inner conductor is connected to the double-loop structure by a microstrip line printed on the front side of the substrate. For the dipole with +45° polarization, the outer conductor of the coaxial line is connected to the double-loop structure by a microstrip line, while the inner conductor is connected to the double-loop structure directly on the front side of the substrate. The structure and dimensions of the antenna were optimized, and the parameters are given in Table 1.

The antenna without the parasitic elements is named as Antenna 1, and the loaded one is named as Antenna 2. To reveal the effect of the parasitic elements, Figure 2 plots the S11 curves of Antenna 1 and Antenna 2, while Figure 3 displays the Z11 curves. It can be seen from the figures that the parasitic elements generate new resonance at lower frequency, which expands the impedance matching band. The parasitic elements also smooth the Z11 curves, and the impedance matching level is improved.

Table 1: Dimensions of the proposed design.

Parameters	Value (mm)
wg	320
Lg	320
ws	200
Ls	200
s	10
*W*1	30
*W*2	62
*L*2	62
*W*3	38
*L*3	38
h	78
*H*0	2

The surface current distribution of Antenna 1 (0.8 GHz) and Antenna 2 (0.54 GHz) is plotted in Figure 4 as port 1 is excited. This shows that the current at 0.8 GHz for Antenna 1 concentrates on the entire dual-loop structure, while the current of Antenna 2 is extended to parasitic elements. The current on the dual-loop structure couples to parasitic elements; thus, the total current path is extended, and the resonance is moved to lower frequency. However, the inductance on the parasitic elements and the capacitance between the ground and the patch generate new resonance at lower frequency, and then, the operating band is extended to lower frequency.

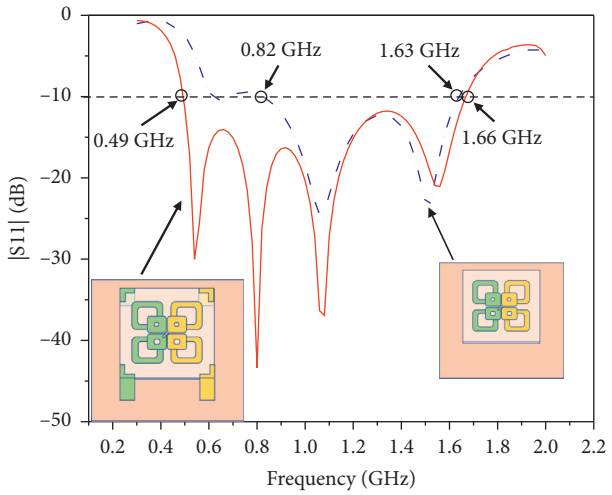

Figure 2: Simulated S-parameters of the antenna with/without parasitic elements.

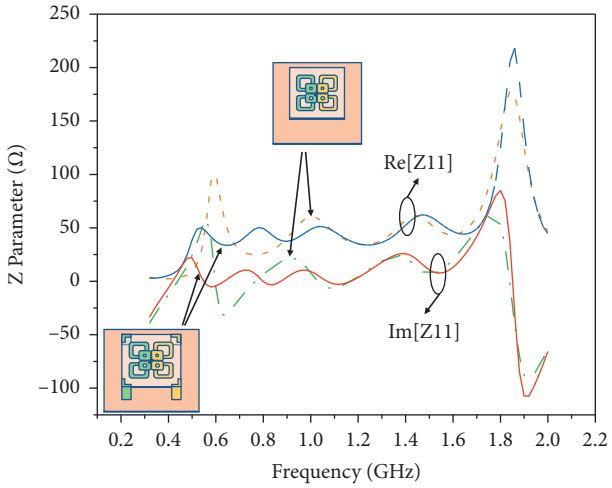

Figure 3: Simulated Z-parameters of the antenna with/without parasitic elements.

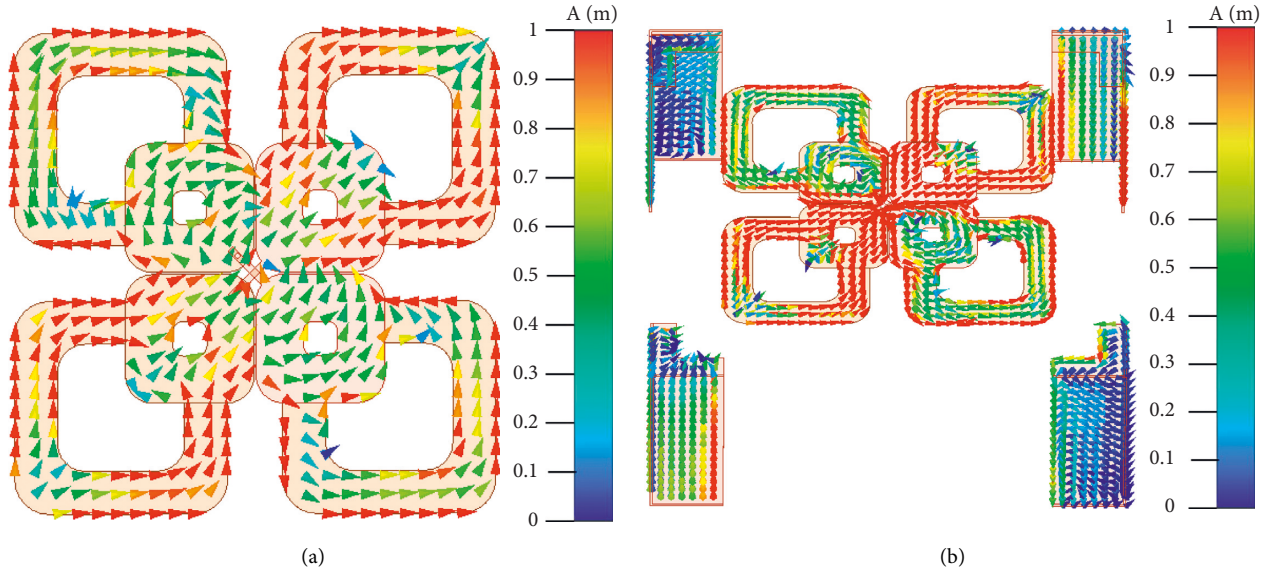

Figure 4: Current distribution. (a) Antenna 1. (b) Antenna 2.

The effect of the distance between the substrate and the ground on S11 is demonstrated in Figure 5. A better impedance bandwidth is obtained with $h = 80$ mm when h is approximately equal to a quarter of the wavelength of the center frequency. The effect of the length of the parasitic patch on S11 is shown in Figure 6, where the optimal result is $w1 = 30$ mm. It can be seen from Figure 7 that impedance matching becomes worse as s increases, so s is set at 80 mm. The effect of ground width on VSWR and the front-to-back ratio is shown in Figure 8. Changing the ground size, the VSWR remains essentially the same, with the front-to-back ratio showing a trend of decreasing and then increasing. The reason may be that, as the frequency increases, the wavelength becomes shorter and the back flap becomes larger. At 0.8–1.6 GHz, narrowing of the beam causes the variation in gain to be greater than the increase in the back flap, so the front-to-back ratio increases. Considering the size and performance of the antenna, Wg is set at 320 mm.

2.2. Operating Principle. The loading of the parasitic elements is equivalent to the introduction of terminal loading at the end of the antenna, as shown in Figure 9. Miniaturization of the antenna can be achieved by reducing the phase velocity of the guided waves on the antenna to create resonance and coherent radiation. At the same time, a good impedance matching of the antenna should be ensured [18]. The phase velocity and the characteristic impedance of the antenna can be given by

$$V_p = \frac{1}{\sqrt{LC}}, \qquad Z_0 = G\sqrt{\frac{L}{C}}, \tag{1}$$

where L is the series inductance per unit length of the antenna, C is the shunt capacitance per unit length of the antenna, and G is a geometrical factor. It means that the series inductance and the parallel capacitance of the antenna structure affect the impedance bandwidth and antenna size. The introduction of the L-shaped patch and the metallic plate makes the dipole more inductive, and the L-shaped patch and the ground are equivalent to a capacitor (the distance between the patch and ground is only 0.13λ, λ is the free-space wavelength at 500 MHz), resulting in better impedance matching. R is the radiation resistance. It is well known that the resistance is minimum for series resonance and maximum for parallel resonance [14], while the loading of the parasitic elements extends the electrical length of the dipole, we can simplify parasitic elements as parallel resonance at 0.54 GHz and series resonance at 0.8 GHz.

The equivalent circuit in Figure 9 is derived, and the results are compared in Figure 10. As can be seen from Figure 10, the resonance characteristics of Antenna 1 with the circuit loading and Antenna 2 roughly agree with each other. The optimized parameters are $L_a = 11.9$pF, $C_a = 1.6$ nH, $L_b = 25$ nH, $C_b = 1.0$ pF, and $R_c = 25\ \Omega$.

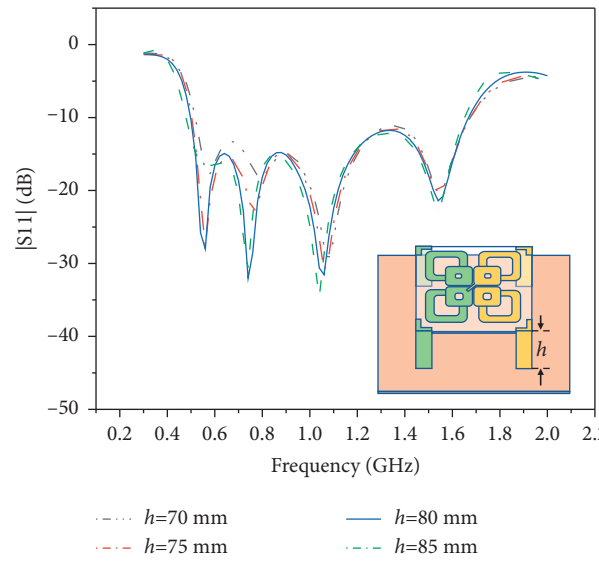

Figure 5: Effect of the distance (h) between the substrate and the ground on S11.

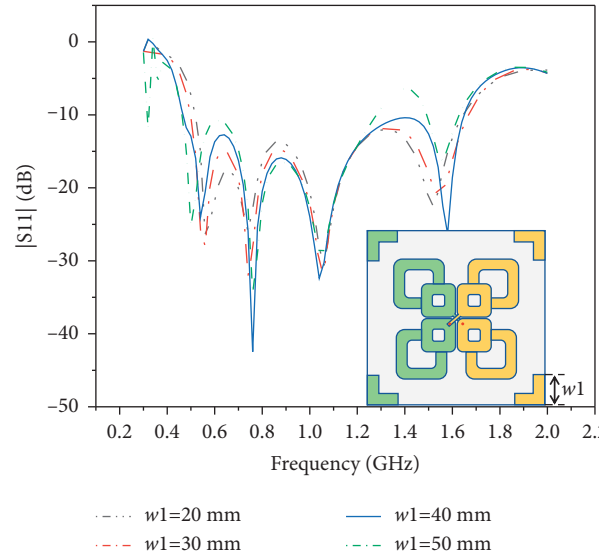

Figure 6: Effect of the length ((w)1) of the parasitic patch on S11.

3. Antenna Measurement Results

A prototype of the proposed antenna is fabricated as shown in Figure 11. The simulated and measured results of the S-parameters are given in Figure 12. As can be seen from the figure, the measured and simulated results are basically consistent, and the discrepancies may be caused by the low accuracy of the manual welding of an aluminum alloy. As the feeding of the two ports is not identical, the relative bandwidth of port 1 is 109.2% (0.54–1.84 GHz) and the relative bandwidth of port 2 is 106.9% (0.5–1.65 GHz), and the overlapping bandwidth between the two ports is 101.4% (0.54–1.65 GHz), while the port isolation is larger than 22 dB, and the minimum isolation is 56.8 dB at 0.5 GHz. Due to the symmetry of the dipoles, only the normalized

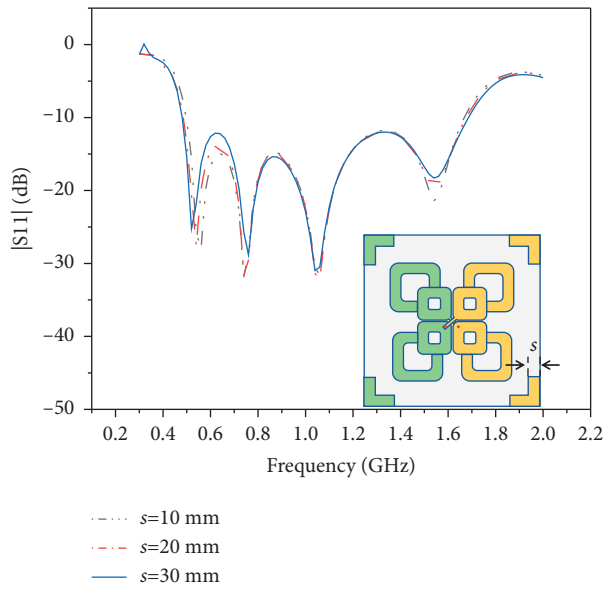

Figure 7: Effect of the width (s) of the parasitic patch on S11.

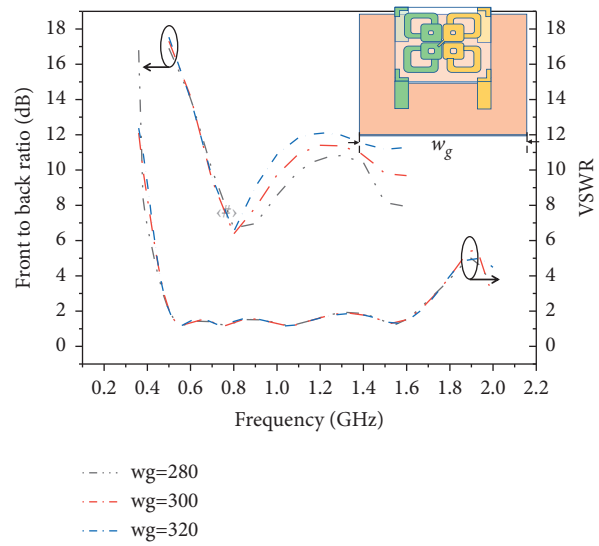

Figure 8: Effect of the ground width (Wg) on the VSWR and the front-to-back ratio.

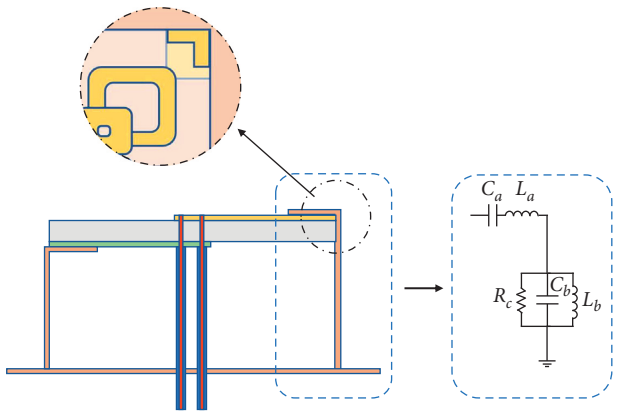

Figure 9: Equivalent circuit diagram of parasitic elements.

radiation pattern of the E-plane for +45° polarization is given in Figure 13. It can be seen from the figure that the antenna can retain good unidirectional radiation characteristics at 0.5 GHz–1.6 GHz with cross-polarization greater than 20 dB. The realized gain of the proposed antenna is given in Figure 14. The realized gain of the proposed antenna is stable at 0.5–0.8 GHz but increases with frequency at 0.8–1.2 GHz, which is due to the narrowing of the beamwidth of the radiation pattern. The reason for the gain of the proposed antenna decrease at 1.2–1.6 GHz is that the backward-radiated electromagnetic wave of the antenna is not superimposed with the forward-radiated electromagnetic wave in the same phase, resulting in distortion of the radiation pattern. It can be seen from Figure 13 that the sidelobe level in the high frequency radiation pattern becomes

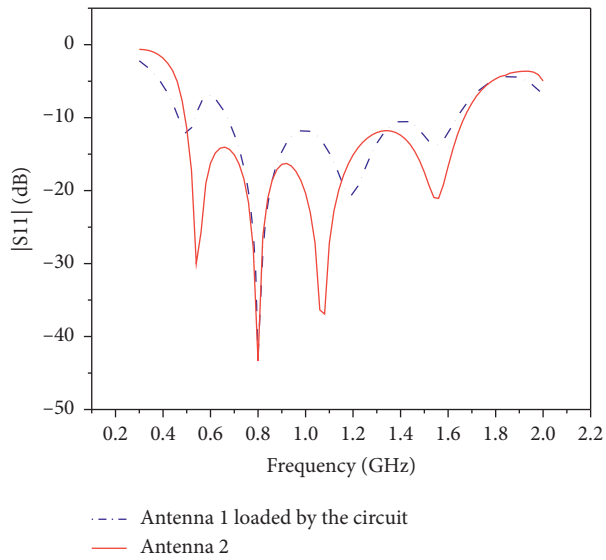

Figure 10: Comparison of S11 between Antenna 1 loaded by the circuit and Antenna 2.

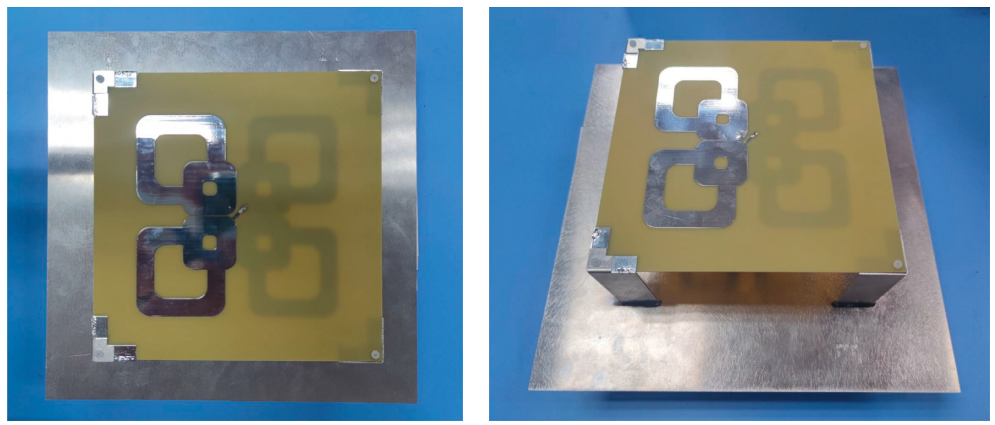

Figure 11: Prototype of the proposed antenna. (a) Top view. (b) Perspective view.

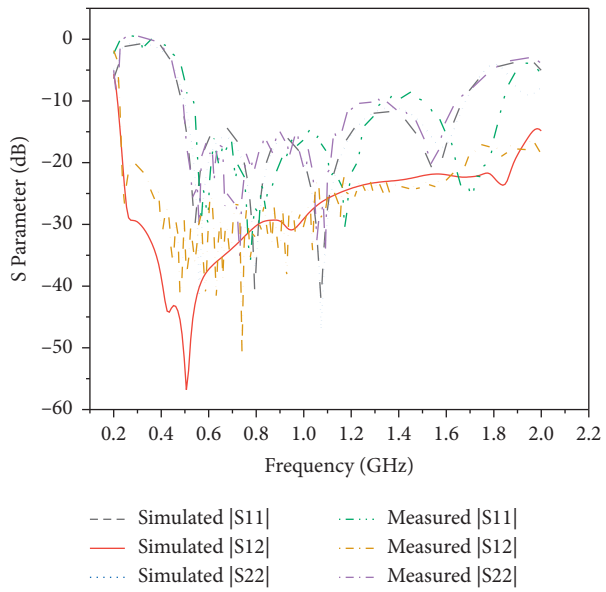

Figure 12: Simulated and measured S-parameters of the proposed antenna.

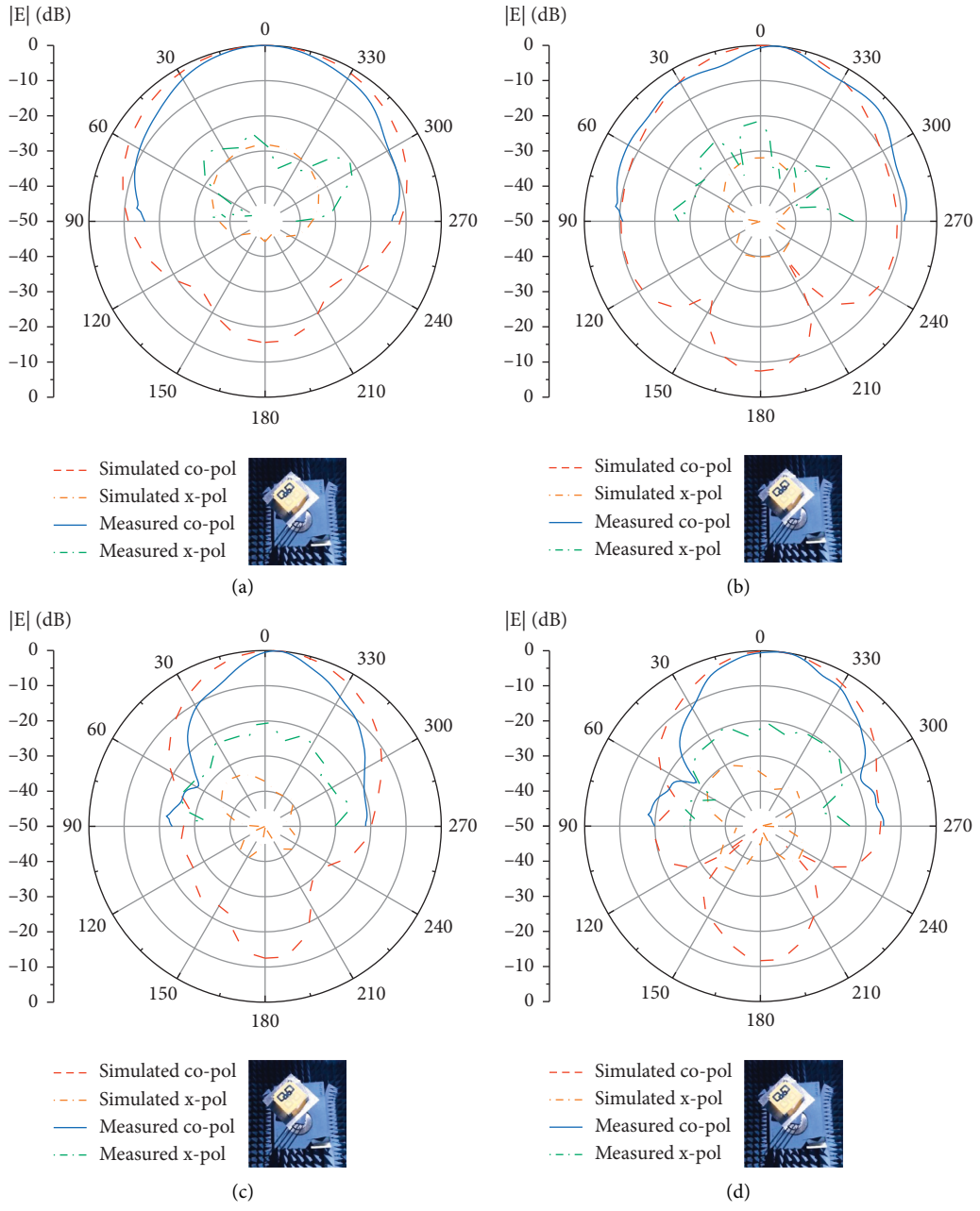

Figure 13: Continued.

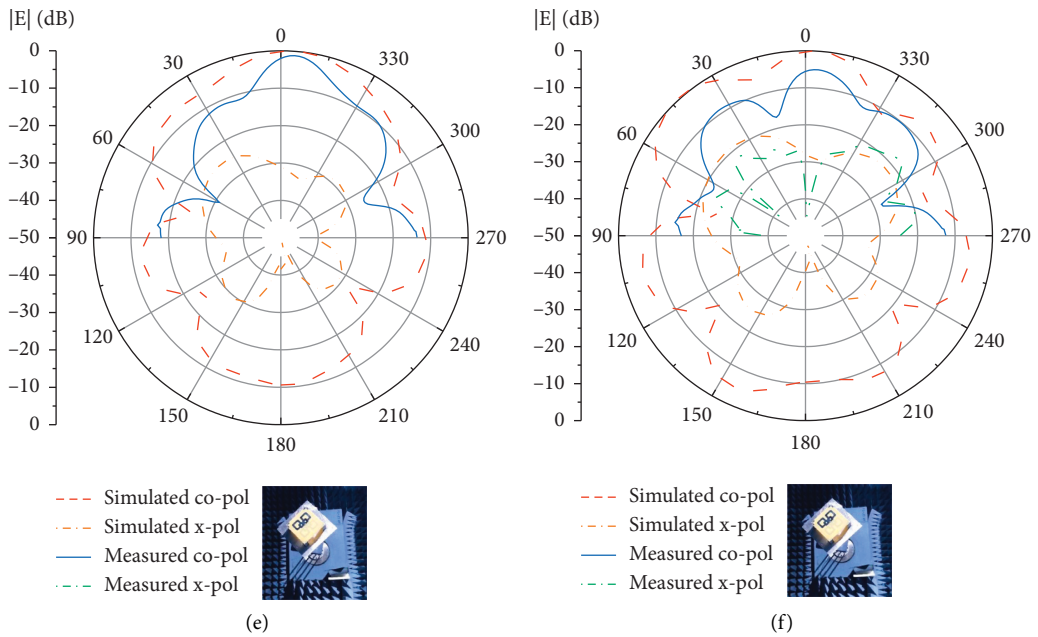

Figure 13: Simulated and measured normalized radiation patterns of the proposed antenna. (a) 0.5 GHz. (b) 0.9 GHz. (c) 1.3 GHz. (d) 1.4 GHz. (e) 1.5 GHz. (f) 1.6 GHz.

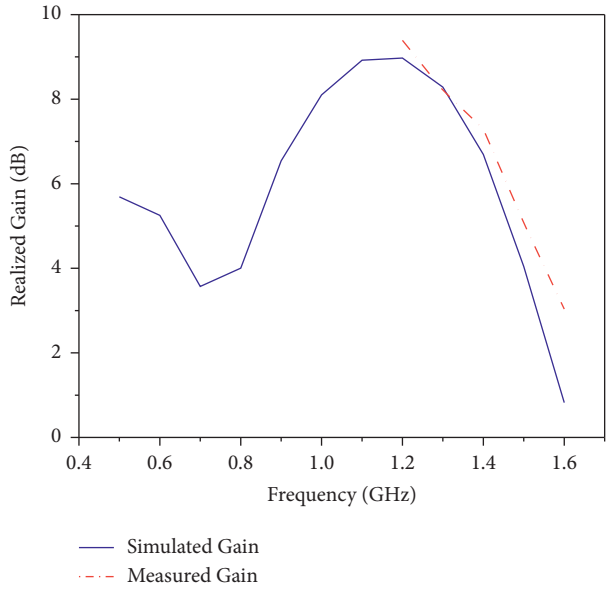

Figure 14: Simulated and measured realized gains of the proposed antenna.

significantly larger. As the given gain of the standard horn starts from 1.1 GHz, the gains of the proposed antenna below 1.1 GHz were not measured. It must be pointed out that the radiation pattern can be measured in the 0.5–1.6 GHz band because the pattern is normalized.

Comparison between the proposed antenna and the reported antennas is shown in Table 2. It is found that the proposed antenna has a smaller size and wider operating bandwidth. The proposed antenna has moderate isolation.

Table 2: Comparison with reported wideband dual-polarized antennas.

Ref	Size	BW	Innovation	ISO	Design difficulty
[2]	$0.36\ \lambda_0 * 0.36\ \lambda_0 * 0.2\ \lambda_0$	45% (1.7–2.7 GHz)	Bow-tie dipole	>30	Low
[3]	$0.37\ \lambda_0 * 0.37\ \lambda_0 * 0.16\ \lambda_0$	65.9%% (1.71–3.4 GHz)	Γ– shaped feeding	>36	Low
[8]	$0.4\ \lambda_0 * 0.4\ \lambda_0 * 0.087\ \lambda_0$	32.7% (0.69–0.96 GHz)	Nonuniform metasurface	>30	High
[9]	$0.4\ \lambda_0 * 0.4\ \lambda_0 * 0.15\ \lambda_0$	22.7% (0.57–0.72 GHz)	Short pins to improve isolation	>35	Low
[10]	$0.39\ \lambda_0 * 0.39\ \lambda_0 * 0.13\ \lambda_0$	38.7%% (1.69–2.5 GHz)	Stepped impedance slot	>35	Low
[11]	$0.34\ \lambda_0 * 0.34\ \lambda_0 * 0.17\ \lambda_0$	48% (1.68–2.74 GHz)	Balun feeding	>22	High
[12]	$0.22\ \lambda_0 * 0.22\ \lambda_0 * 0.17\ \lambda_0$	52.6% (0.63–1.08 GHz)	Differential feeding	>3.15	High
[13]	$0.33\ \lambda_0 * 0.33\ \lambda_0 * 0.16\ \lambda_0$	46.5% (1.7–2.73 GHz)	Short pins to improve isolation	>38	Middle
[15]	$0.38\ \lambda_0 * 0.38\ \lambda_0 * 0.21\ \lambda_0$	67% (1.39–2.8 GHz)	Load parasitic element	>30	High
[16]	$0.52\ \lambda_0 * 0.52\ \lambda_0 * 0.14\ \lambda_0$	90.9% (0.93–2.48 GHz)	Load folded metallic plates	>20	Low
Proposed	$0.36\ \lambda_0 * 0.36\ \lambda_0 * 0.14\ \lambda_0$	101.4% (0.54 GHz–1.65 GHz)	Load L-shaped metallic shorting wall	>22	Low

λ_0: wavelength at the lowest operating frequency.

4. Conclusion

In this paper, a +45°/−45° dual-polarized antenna loaded with parasitic elements is proposed. The introduction of the parasitic elements generates a new resonant mode in the lower frequency band and finally achieves a relative bandwidth of 109.2% for port 1 and 106.9% for port 2, with isolation larger than 22 dB. The antenna obtains good radiation characteristics at 0.5–1.6 GHz with cross-polarization greater than 20 dB. The antenna mentioned in this paper has a smaller size and wider operating bandwidth compared with literature reports, offering a potential choice for base station systems.

Data Availability

The data used to support the findings of this study are included within the article.

Conflicts of Interest

The authors declare that they have no conflicts of interest.

Acknowledgments

This work was supported in part by the Guangxi Natural Science Foundation (2021JJA170177), the Innovation Project of GUET Graduate Education (2022YCXS040), and the Guangxi Key Laboratory of Wireless Wideband Communication and Signal Processing (GXKL06200111).

References

[1] K. Ghaemi and N. Behdad, "A low-profile, vertically polarized ultrawideband antenna with monopole-like radiation characteristics," *IEEE Transactions on Antennas and Propagation*, vol. 63, no. 8, pp. 3699–3705, 2015.

[2] Y. H. Cui, R. L. Li, and H. Z. Fu, "A broadband dual-polarized planar antenna for 2G/3G/LTE base stations," *IEEE Transactions on Antennas and Propagation*, vol. 62, no. 9, pp. 4836–4840, 2014.

[3] B. Q. Bi Qun Wu and K. Kwai-Man Luk, "A broadband dual-polarized magneto-electric dipole antenna with simple feeds," *IEEE Antennas and Wireless Propagation Letters*, vol. 8, pp. 60–63, 2009.

[4] B. Feng, H. Li, K. L. Chung, C. Y. D. Sim, and L. Deng, "A dual-polarized wideband ceiling-mount antenna with low gain variations and high isolation for 5G Sub-6 GHz applications," *IEEE Transactions on Antennas and Propagation*, p. 1, 2022.

[5] B. Feng, Y. Tu, J. Chen, S. Yin, and K. L. Chung, "Dual linearly-polarized antenna array with high gain and high isolation for 5G millimeter-wave applications," *IEEE Access*, vol. 8, Article ID 82471, 2020.

[6] I. A. Osaretin, A. Torres, and C. C. Chi-Chih Chen, "A novel compact dual-linear polarized UWB antenna for VHF/UHF applications," *IEEE Antennas and Wireless Propagation Letters*, vol. 8, pp. 145–148, 2009.

[7] H. Raza, A. Hussain, J. Yang, and P. S. Kildal, "Wideband compact 4-port dual polarized self-grounded bowtie antenna," *IEEE Transactions on Antennas and Propagation*, vol. 62, no. 9, pp. 4468–4473, 2014.

[8] H. Zhu, Y. Qiu, and G. Wei, "A broadband dual-polarized antenna with low profile using nonuniform metasurface," *IEEE Antennas and Wireless Propagation Letters*, vol. 18, no. 6, pp. 1134–1138, 2019.

[9] S. G. Shi-Gang Zhou, P. K. Peng-Khiang Tan, and T. H. Tan-Huat Chio, "Low-profile, wideband dual-polarized antenna with high isolation and low cross polarization," *IEEE Antennas and Wireless Propagation Letters*, vol. 11, pp. 1032–1035, 2012.

[10] R. Lian, Z. Wang, Y. Yin, J. Wu, and X. Song, "Design of a low-profile dual-polarized stepped slot antenna array for base station," *IEEE Antennas and Wireless Propagation Letters*, vol. 15, pp. 362–365, 2016.

[11] H. Huang, Y. Liu, and S. Gong, "A broadband dual-polarized base station antenna with sturdy construction," *IEEE Antennas and Wireless Propagation Letters*, vol. 16, pp. 665–668, 2017.

[12] C. Zhou, L. Guo, H. Sun, and M. LiLi, "A wideband dual polarized dual-mode antenna with simple differential feeding," *IEEE Antennas and Wireless Propagation Letters*, vol. 19, no. 10, p. 1, 2020.

[13] B. Li and Y. Z. Yin, "Wideband dual-polarized patch antenna with low cross polarization and high isolation," *IEEE Antennas and Wireless Propagation Letters*, vol. 11, pp. 427–430, 2012.

[14] Z. Li, J. Han, Y. Mu, X. Gao, and L. Li, "Dual-band dual-polarized base station antenna with a notch band for 2/3/4/5G communication systems," *IEEE Antennas and Wireless Propagation Letters*, vol. 19, no. 12, pp. 2462–2466, 2020.

[15] Y. Cui, L. Wu, and R. Li, "Bandwidth enhancement of a broadband dual-polarized antenna for 2G/3G/4G and IMT base stations," *IEEE Transactions on Antennas and Propagation*, vol. 66, no. 12, pp. 7368–7373, 2018.

[16] W. Yang and Y. Pan, "A wideband dual-polarized dipole antenna with folded metallic plates," *IEEE Antennas and Wireless Propagation Letters*, vol. 17, no. 10, pp. 1797–1801, 2018.

[17] H. Bai, J. Guo, and A. Feng, "A Broadband Low-Profile Dual-Polarized Antenna," in *Proceedings of the 2019 International Symposium On Antennas And Propagation*, pp. 1-2, Xi'an, China, October 2019.

[18] B. A. Kramer, C. C. Chen, M. Lee, and J. L. Volakis, "Fundamental limits and design guidelines for miniaturizing ultra-wideband antennas," *IEEE Antennas and Propagation Magazine*, vol. 51, no. 4, pp. 57–69, 2009.